Pharmacological control of CAR T cells through CRISPR-driven rapamycin resistance

Sébastien Levesque[1,2,3], Gillian Carleton[4,5], Victoria Duque[1,2], Claudia Goupil[1,2], Jean-Philippe Fiset[1,2], Sarah Villeneuve[1,2], Eric Normandeau[6], Geneviève Morin[6], Nellie Dumont[7], Brad H. Nelson[4,5], Josée Laganière[7], Brian Boyle[6], Julian J. Lum[4,5], Yannick Doyon[1,2*]

[1]Centre Hospitalier Universitaire de Québec Research Center - Université Laval, Québec, QC, G1V 4G2, Canada.
[2]Université Laval Cancer Research Centre, Québec, QC, G1V 0A6, Canada.
[3]Present Address: Division of Hematology/Oncology, Boston Children's Hospital. Department of Pediatric Oncology, Dana-Farber Cancer Institute. Harvard Stem Cell Institute. Broad Institute of MIT and Harvard. Department of Pediatrics, Harvard Medical School, Boston, MA 02115, USA.
[4]Trev and Joyce Deeley Research Centre, BC Cancer, Victoria, BC, V8R 6V5, Canada.
[5]Department of Biochemistry and Microbiology, University of Victoria, Victoria, BC, V8P 5C2, Canada.
[6]Institut de Biologie Intégrative des Systèmes, Université Laval, Québec, QC, G1V 0A6.
[7]Medical Affairs and Innovation, Héma-Québec, Québec, Quebec, Canada

[*]Correspondence:
Yannick Doyon, Ph.D.
Centre de recherche du CHU de Québec – Université Laval
2705, boulevard Laurier, T-3-67
Québec, QC G1V 4G2
CANADA

Tel: 418-525-4444 ext. 46264
e-mail: Yannick.Doyon@crchudequebec.ulaval.ca
ORCID 0000-0002-3889-9563

ABSTRACT

Chimeric antigen receptors (CARs) reprogram T cells to recognize and target cancer cells. Despite remarkable responses observed with CAR-T cell therapy in patients with hematological malignancies, CAR-T cell engineering still relies mostly on randomly integrating vectors, limiting the possibilities of fine-tuning T cell function. Here, we designed a CRISPR-based marker-free selection strategy to simultaneously target a therapeutic transgene and a gain-of-function mutation to the *MTOR* locus to enrich cells resistant to rapamycin, a clinically used immunosuppressant. We readily engineered rapamycin-resistant (RapaR) CAR-T cells by targeting CAR expression cassettes to the *MTOR* locus. Using *in vitro* cytotoxicity assays, and a humanized mouse model of acute lymphoblastic leukemia, we show that RapaR-CAR-T cells can efficiently target CD19^{+} leukemia cells in presence of immunosuppressing doses of rapamycin. Furthermore, our strategy allows multiplexed targeting of rapamycin-regulated immunoreceptors complexes (DARICs) to the *MTOR* and *TRAC* loci to pharmacologically control CAR-T cells' activity. We foresee that our approach could both facilitate the enrichment of CRISPR-engineered CAR-T cells *ex vivo* and *in vivo* while improving tumor eradication.

INTRODUCTION

Adoptive cell therapy with chimeric antigen receptor T (CAR-T) cells has shown remarkable potency against relapsed and refractory acute lymphoblastic leukemia (ALL) and non-Hodgkin lymphoma[1–5]. CAR-T cells are genetically engineered T cells that are able to recognize and target cancer cells expressing a specific antigen on their surface[6,7]. Randomly integrating vectors based on retroviruses, lentiviruses or *piggyBac* transposons are routinely used for cell therapy applications, but genome editing technologies offer a wide a range of opportunities to enhance CAR-T cells functionality[8,9]. The promising potential of CRISPR-based technologies to engineer CAR-T cells has been demonstrated by targeting a CAR to the *TRAC* locus to avert tonic CAR signaling and delay T cells differentiation and exhaustion[10], or by generating HLA-independent T cell receptors (HIT) to afford high antigen sensitivity[11]. CRISPR-based technologies also offer great potential to inactivate key genes involved in T cells dysfunction[12–14] or to generate allogeneic universal CAR-T cells[15–17].

While progress has been made towards high-yield targeted transgene integration in primary cells[10,11,18], enrichment strategies could further facilitate the development of CRISPR-engineered cell therapies. To enrich targeted transgene integration via homology-directed repair (HDR) in primary T cells, a selection method based on the expression of a methotrexate-resistant dihydrofolate reductase mutant has previously been reported[19]. A metabolic safety switch has also been developed via *UMPS* knockout to enrich T cells expressing reporter transgenes[20]. However, no marker-free selection strategy has been developed to simultaneously enrich CRISPR-engineered CAR-T cells and enhance their antitumor activity.

The serine/threonine protein kinase mTOR constitutes the catalytic subunit of two distinct complexes, known as mTORC1 and mTORC2, which coordinate eukaryotic cell growth and metabolism by integrating a diverse set of environmental inputs[21–23]. mTORC1 controls cellular growth and metabolism by sensing nutrient levels and growth factor signals to coordinate anabolic and catabolic metabolism[24]. While mTORC1 is sensitive to rapamycin, an immunosuppressant also used in oncology, mTORC2 remains functional upon acute rapamycin treatment[21–23]. Considering that mTOR signaling is commonly activated in tumor cells and alters the expression and the activity of key metabolic enzymes[21,25,26], combinatorial CAR-T cell therapy with rapamycin could synergistically enhance antitumor activity. Indeed, random integration of a rapamycin-resistant mTOR transgene and a CD19-CAR in primary T cells using *piggyBac* transposons has been shown to confer a selective growth advantage in the presence of rapamycin and enhanced antitumor activity when used in combination[27]. However, delivery of this large transgene is limiting, and product-derived lymphomas have been reported with *piggyBac*-modified CAR-T cells[28,29], so editing the endogenous *MTOR* locus to generate dominant cellular resistance to rapamycin using CRISPR could be a viable alternative. Since mTORC1 signaling lies downstream of several activation signals essential for T cell activation and expansion[21,30], this central signaling node is a prime target to develop a tissue-specific marker-free selection strategy for CRISPR-engineered CAR-T cells. More importantly, CRISPR-induced drug resistance offers great potential for pharmacological control of CAR-T cells activity through receptor dimerization[31,32] even when using an immunosuppressive dose of rapamycin.

91 In this study, we performed saturation prime editing[33] at the *MTOR* locus to identify and
92 characterize optimal mutations conferring rapamycin resistance. We then devised an intron nesting
93 strategy[34,35] to enrich CRISPR-engineered cells *ex vivo* and *in vivo* without using an exogenous
94 selection marker. We demonstrate that targeting CAR expression cassettes to the *MTOR* locus
95 allows the selection and regulation of rapamycin-resistant CAR-T cells to perform combinatorial
96 immunotherapy with rapamycin. More broadly, we propose a versatile approach to facilitate
97 targeted therapeutic transgene integration for cell therapy applications.
98

99 # RESULTS

100 **Identification and characterization of mutations conferring rapamycin resistance via**
101 **saturation prime editing**

102 After an extraordinary 18-month response to everolimus, a rapamycin analog, a patient with
103 metastatic anaplastic thyroid carcinoma relapsed with a resistant tumor harboring the *MTOR*-
104 F2108L mutation[36]. The same mutation was also found in spontaneous rapamycin-resistant yeast
105 mutants[37], and a clonal MCF-7 breast cancer cell line after three months of exposure to
106 rapamycin[38]. Of importance, this mutation does not hyperactivate mTOR[34,36,38] and confers
107 resistance to first-generation allosteric inhibitors of mTOR, but not to second- and third-generation
108 inhibitors[36,38]. F2108 lies within the FKBP12-rapamycin binding (FRB) domain of mTOR and is
109 an important residue involved in rapamycin interactions[39]. We performed saturation mutagenesis
110 of F2108 to install all possible amino acids substitutions at the endogenous *MTOR* locus to identify
111 and characterize alternative mutations causing rapamycin-resistance at this position. We devised
112 a saturation prime editing (PE) screen[33] using K562 cells stably expressing the mScarlet-I mTOR
113 signaling indicator (mSc-TOSI)[34,40] as a phenotypic readout to interrogate the functional impact of
114 these mutations (**Fig. 1a,b** and **Supplementary Fig. 1**). Under active mTORC1 signaling, the
115 fluorescent mSc-TOSI reporter is rapidly phosphorylated by S6K, ubiquitinated, and degraded by
116 the proteasome while mTOR inhibition stabilizes the reporter (**Fig. 1b**)[34,40].
117

118 We transfected our reporter cell line with a library of engineered pegRNA (epegRNA)[41] encoding
119 F2108 variants and performed rapamycin selection starting 3 days post-transfection until all non-
120 resistant cells were eliminated. Selection was performed at 0.5 μM rapamycin, the lowest
121 concentration of this drug that strongly abrogates K562 cell proliferation under our growth

122 conditions. We performed high-throughput sequencing prior and after FACS-based cell sorting
123 and analyzed the fold enrichment of all possible *MTOR*-F2108 permutations (**Fig. 1c,d** and
124 **Supplementary Fig. 1**). The most enriched mutation was F2108L[36,38] (4.8 fold enrichment), but
125 five additional mutations displaying 1.6 to 2.3 fold enrichments were selected for further
126 characterization (**Fig. 1d**). Of importance, cells modified at *MTOR* remained sensitive to the 2nd
127 generation ATP-competitive inhibitor AZD8055[42], which could be used as a safety switch in case
128 of overt toxicity (**Fig. 1c** and **Supplementary Fig. 1** and **2**).
129
130 To validate the top hits, we designed epegRNAs to test these variants individually. K562 cells
131 harboring these *MTOR*-F2108 substitutions grew robustly in the presence of 0.5 μM rapamycin
132 and we observed a marked increase in the percentage of alleles harboring the PE-specified edits
133 after rapamycin selection (**Supplementary Fig. 1**). As expected, no resistance and no enrichment
134 were observed with the silent F2108F mutation (**Supplementary Fig. 1**). These observations
135 confirmed that the five new variants identified by saturation prime editing conferred dominant
136 cellular resistance to rapamycin. Furthermore, mTORC1 signaling remained fully functional with
137 the F2108L mutation but was completely blocked with the silent F2108F mutation
138 (**Supplementary Fig. 1 and 2**). However, intermediate levels of signaling in the presence of
139 rapamycin were observed with F2108I, F2108M, and F2108G while weak activity was observed
140 with F2108V and F2108K (**Supplementary Fig. 1 and 2**). These observations suggest that robust
141 K562 cell growth can be maintained with partial mTORC1 signaling. These *MTOR*-F2108
142 mutations could potentially be used to pharmacologically fine-tune mTORC1 signaling while
143 maintaining robust cellular growth. Overall, mTORC1 signaling remains completely functional in
144 the presence of rapamycin with F2108L, and this mutation was selected to develop a marker-free
145 selection strategy to engineer rapamycin-resistant CAR-T cells.
146
147 **Concomitant transgene integration and induction of rapamycin resistance by nuclease-**
148 **driven *MTOR* editing in primary T cells.**
149 While creating F2108L by itself via PE could be used to potentiate CAR-T cells, we aimed to
150 determine if we could couple rapamycin resistance to transgene integration in a single step by
151 editing the *MTOR* locus via homology-directed repair (HDR). As we previously showed for the
152 essential *ATP1A1* gene[34], this strategy can work by nesting a transgene within an intron without

153 disrupting the recipient gene[34,35]. We first designed two sgRNAs targeting *MTOR* intron 45 in
154 proximity to F2108 using CRISPOR[43] (see G4 and G5 in **Fig. 1a**). These two chemically modified
155 sgRNAs generated 86-90% indels in primary T cells when delivered as RNPs with both SpCas9
156 and the high-fidelity variant HiFiCas9[44] (**Fig. 2a**). To assess their genome-wide specificity, we
157 performed GUIDE-Seq[45,46] in primary $CD3^+$ T cells from two healthy donors using wild-type
158 SpCas9. While 9 potential off-target sites were identified with *MTOR*-G5, only one was identified
159 with *MTOR*-G4 in $CD3^+$ T cells (**Fig. 2b** and **Supplementary Fig. 3**). Similar results were
160 obtained in K562 cells via plasmid overexpression (**Supplementary Fig. 3**). We then performed
161 RNPs nucleofection in $CD3^+$ T cells from two healthy donors followed by amplicon sequencing to
162 validate GUIDE-Seq off-targets and test whether HiFiCas9 could mitigate off-target activity.
163 While the frequency of alleles with indels above the 0.1% limit of detection was observed at all
164 off-targets with SpCas9, HiFiCas9 abrogated off-target editing at all off-targets except *MTOR*-G5
165 OT1 (**Fig. 2c**). Since *MTOR*-G4 is highly active and specific, we prioritized this sgRNA for our
166 studies.
167
168 Next, using Cas9 RNPs and PCR-generated linear dsDNA donors[47], we confirmed that rapamycin
169 resistance could be achieved in primary $CD3^+$ T cells and observed a marked increase to up to
170 62% of alleles harboring the *MTOR*-F2108L mutation after selection (**Supplementary Fig. 4**).
171 This increase in HDR in the population upon selection was concomitant with a decrease of indels
172 detected at the cut site, suggesting efficient elimination of cells not having undergone HDR
173 (**Supplementary Fig. 4**). No enrichment was observed when using a donor that harbored the
174 wildtype *MTOR*-F2108 codon, confirming that robust growth in the presence of rapamycin
175 depends on the *MTOR*-F2108L mutation (**Supplementary Fig. 4**). In these experiments, a dose of
176 25 nM rapamycin was chosen based on growth curves indicating that maximal inhibition occurred
177 in the 16-32 nM range under our conditions (data not shown). A similar dose was used in previous
178 studies[27] and it falls between the immunosuppressive window of 3-22 nM and the maximal steady-
179 state plasma drug concentrations observed in clinical settings[31,48]. Thus, the installation of the well-
180 characterized *MTOR*-F2108L mutation[36,38] via HDR confers dominant cellular resistance to
181 rapamycin in primary T cells.
182

183 We then devised the strategy to simultaneously target a therapeutic transgene and introduce the
184 F2108L mutation to the *MTOR* locus (**Fig. 3a**). After targeted integration, *MTOR*-F2108L is
185 expressed on the forward DNA strand while the moderately active human *PGK1* promoter drives
186 the expression of a therapeutic transgene of interest on the reverse DNA strand (**Fig. 3a**). As a first
187 test, we targeted an expression cassette encoding the fluorescent protein mScarlet-I to the *MTOR*
188 locus in $CD3^+$ T cells using linear dsDNA donors[47]. Rapamycin selection reproducibly doubled
189 targeted integration frequency and we observed up to 31% of cells expressing the nested reporter
190 transgene (**Supplementary Fig. 5**). Similarly, we achieved 11% knock-in efficacy of a CD19-
191 CAR-2A-EGFP gene cassette (4.6 kb) following treatment for 8 days with rapamycin
192 (**Supplementary Fig. 6**). While encouraging, the use of large linear dsDNA donor caused toxicity,
193 limited proliferation, and was generally prohibitive for highly efficient gene targeting[47]. In
194 addition, these experiments were performed with $CD3^+$ T cells retained in leukoreduction system
195 (LRS) chambers that are typically discarded by blood banks. We found that these cells have higher
196 death rates and limited growth potential under our genome editing conditions in contrast to cells
197 isolated from whole blood donations. Nevertheless, taken together, these data illustrate that
198 rapamycin resistant primary T cells can be engineered to express transgenes in a single homology-
199 directed step using CRISPR-Cas9.
200
201 **One-step generation of rapamycin resistant CAR-T cells**
202 To improve targeting efficacy, we delivered the CD19-CAR-2A-EGFP donor using an adeno-
203 associated virus 6 (AAV6) vector[10,11,20] (**Fig. 3a**). Following Cas9 RNP nucleofection, $CD3^+$ T
204 cells isolated from whole blood (Donor ID: WB 1) were transduced with the AAV6 vector in a
205 small volume for 8 hours and then transferred to the culture medium for three days before
206 rapamycin treatment. Cells were reactivated four days post-transfection and expanded for an
207 additional 7 days before quantification of transgene-expressing cells (**Fig. 3b**). We observed a
208 substantial increase in editing efficacy both pre and post 8 days of selection as determined by out-
209 out PCR and Sanger sequencing in the bulk populations (**Fig. 3c**). Yields of CAR-2A-$EGFP^+$ cells
210 reached 82% and 85% at MOIs of $5x10^3$ and $1x10^4$, respectively as determined by FACS-based
211 analysis (**Fig. 3d**). These results were reproduced with $CD3^+$ T cells isolated from a second whole
212 blood donor (Donor ID: WB2) and two LRS donors (Donor ID: LRS1, LRS2) (**Fig. 3e**). In total,

213 cells from four distinct healthy donors generated similar outcomes, albeit with lower efficiency
214 when using cells isolated from LRS chambers (**Fig. 3e**).
215
216 To test for functionality, we performed luciferase-based cytotoxicity assays with selected CAR-T
217 effector cells and $CD19^+$ NALM6 target cells stably expressing firefly luciferase and RFP. We
218 also generated a rapamycin-resistant NALM6 cell line (NALM6-RapaR) by installing the *MTOR*-
219 F2108L mutation to assess the combinational impact of rapamycin. We observed high levels of
220 cytotoxicity with and without rapamycin at the highest effector to target ratios (**Fig. 3f**). At lower
221 effector to target ratios, higher levels of cytotoxicity were observed in the presence of rapamycin,
222 confirming that these CAR-T cells can be used in combination with the mTOR inhibitor to target
223 cancer cells (**Fig. 3f**). This combinatorial effect was not observed with NALM6-RapaR cells (**Fig.**
224 **3f**). These data indicate that immunosuppressive doses of rapamycin can be used in combination
225 with these CAR-T cells to increase antitumor activity *in vitro*.
226
227 Rapamycin has previously been shown to accelerate the memory T-cell differentiation program
228 and may impact the phenotype of treated cells[49,50]. To begin to probe the impact of rapamycin
229 treatment *ex vivo*, we analyzed differentiation and exhaustion markers and performed multi-color
230 flow cytometry panels after 8 and 15 days of treatment using $CD3^+$ T cells isolated from whole
231 blood of two additional healthy donors (ID: WB3, WB4) (**Supplementary Fig. 7**). In these
232 experiments, editing rates remained high (~80% CAR-2A-$EGFP^+$ cells) and we observed a
233 minimal impact of rapamycin treatment on the expression of differentiation and exhaustion
234 markers, as determined by CD4, CD8, CD45RO, CCR7, and PD1 staining, on both rapamycin-
235 sensitive and rapamycin-resistant T cells (**Supplementary Fig. 7**). Rapamycin-resistant CAR-2A-
236 $EGFP^+$ populations displayed a mix of central memory ($CCR7^+/CD45RO^+$) and effector memory
237 ($CCR7^-/CD45RO^+$) T cells after 8 days of treatment with rapamycin, while most cells displayed
238 an effector memory ($CCR7^-/CD45RO^+$) phenotype after 15 days of treatment (**Supplementary**
239 **Fig. 7**). Overall, rapamycin treatment (25 nM) had little impact on T cells' differentiation in our
240 *ex vivo* expansion protocol, and our 14 days expansion timeline (8 days of rapamycin treatment)
241 yields a mix of central memory and effector memory CAR-T cells.
242

243 **Combinatorial CAR-T cell therapy with rapamycin slows leukemia progression *in vivo***

244 We then established a xenograft leukemia model using NOD/SCID/IL-2Rγ-null (NSG) male and
245 female mice injected with NALM6 cells stably expressing RFP and firefly luciferase. NALM6
246 cells were injected intravenously, and rapamycin treatment (4 mg/kg, daily) started three days
247 later. Rapamycin-resistant CD19-CAR-2A-EGFP^{+}-CAR T cells (Donor ID: WB2, see **Fig. 3e**),
248 which underwent *ex vivo* selection with 25 nM rapamycin for eight days (see **Fig. 3a,b)** , were
249 administered intravenously four days after tumor inoculation (**Fig. 4a)**. In total, these CD19-CAR
250 T cells where expanded *ex vivo* for 14 days and stimulated twice before being injected in mice (see
251 **Fig. 3b)**. As a negative control, we used CD3^{+} T cells untransduced (UT) with AAV6 donors but
252 having undergone nucleofection with the Cas9-*MTOR*-G4 RNP. Tumor engraftment and
253 progression were assessed via bioluminescence imaging twice per week for seven weeks. While
254 rapid tumor progression was observed with UT T cells without treatment, rapamycin slowed tumor
255 progression and conferred an additional week of survival (**Fig. 4b,c)**. Of importance, rapamycin-
256 resistant CD19-CAR-T cells selected *ex vivo* could efficiently target NALM6 cells *in vivo* in the
257 presence or absence of rapamycin (**Fig. 4b,c)**. Combinatorial rapamycin administration with
258 rapamycin-resistant CAR-T cells further slowed tumor progression and allowed the mice to
259 survive for up to seven weeks post-tumor inoculation (**Fig. 4b,c)**. While we observed antitumor
260 control during the first weeks, tumors eventually rebounded and killed all mice (**Fig. 4b,c)**. Our
261 results corroborate previous findings demonstrating the limited persistence of second-generation
262 CARs harboring a CD28 costimulation domain compared to 4-1BB[51–53]. Indeed, the second-
263 generation CD19-CAR architecture used during this study[54] contains a CD28 transmembrane
264 domain, which can form an heterodimer with CD28[55], and a CD28 costimulation domain that has
265 been linked to lower persistence compared to 4-1BB[6,53,56]. Nevertheless, our results confirmed that
266 our targeting strategy can create functional rapamycin-resistant CAR-T cells that can be used in
267 combination with rapamycin to slow tumor progression *in vivo*, offering an opportunity to target
268 cancer cells' metabolism to facilitate tumor eradication.

269

270 **Pharmacological control of CAR-T cell activity using rapamycin**

271 Using intracellular[32] or extracellular[31] rapamycin-regulated dimerization domains to
272 pharmacologically control chimeric antigen receptor assembly is a promising approach for
273 developing safer CAR-T cell therapies[57]. However, these systems rely on the non-

274 immunosuppressive rapamycin analog AP21967 which was primarily developed as a tool for
275 chemical biology and do not have suitable pharmacokinetic properties for clinical use[32], or on non-
276 immunosuppressive doses of rapamycin, which limit their clinical potential. Thus, we tested
277 whether we could target a dimerizing agent-regulated immunoreceptor complex (DARIC)[31], which
278 can be toggled between on and off states using rapamycin, to the *MTOR* locus.
279
280 Building on previous studies[10,31], we sought to test whether multiplexed targeting of separate
281 DARIC components could be performed at the *MTOR* and *TRAC* loci simultaneously (**Fig. 5a**).
282 Taking advantage of the dynamic regulation of CAR expression at the *TRAC* locus[10], which averts
283 tonic CAR signaling, we targeted a CD22 recognition domain (DARIC 2) and a 41BB-CD3z
284 signaling domain (DARIC 3) linked by a P2A self-cleaving peptide to the *TRAC* locus (**Fig. 5a**).
285 In parallel, we targeted an additional CD19 recognition domain (DARIC 1) to the *MTOR* locus to
286 confer dominant cellular resistance to rapamycin while providing an additional antigen specificity
287 to potentially overcome antigen escape[6,7,56,58,59]. Multiplexed targeted integration of both DARIC
288 cassettes was observed at *MTOR* and *TRAC*, as determined by out-out PCR (**Fig. 5b**). An average
289 of 58% of alleles harboring the *MTOR*-F2108L was observed, confirming that multiplexed genome
290 editing did not decrease targeted transgene integration at *MTOR* (**Fig. 5b**). We performed FACS-
291 based cytotoxicity assays using unselected CAR-T cells in the presence or absence of 25 nM
292 rapamycin with DARIC-T cells that were resistant (RapaR-CD19-CD22-DARIC) or not (CD22-
293 DARIC) to rapamycin. Strikingly, cytotoxicity was only observed with rapamycin-resistant CD19-
294 CD22-DARIC-T cells in the presence of rapamycin, confirming DARIC immunoreceptor
295 dimerization only in the presence of the drug (**Fig. 5c**). As observed above, rapamycin inhibited
296 NALM6 cell growth to some extent, but not NALM6-RapaR which harbors the *MTOR*-F2108L
297 mutation (**Fig. 5c**). Rapamycin-sensitive CD22-DARIC-T cells, where the *MTOR*-F2108L-
298 DARIC-1 AAV6 donor was omitted during transduction, could not target cancer cells in the
299 presence of an immunosuppressive dose of 25 nM rapamycin (**Fig. 5c**). We note that the CD22
300 scFv construction (DARIC 2) we engineered has never been tested for functionality by itself, thus
301 the absence of cytotoxicity of CD22-DARIC cells in presence of rapamycin should be interpreted
302 with caution.
303

304 Using our established xenograft leukemia model, we then tested whether multiplexed DARIC
305 targeting could be used to activate DARIC-T cells *in vivo* even when using an immunosuppressive
306 dose of rapamycin. We targeted DARIC components to the *MTOR* and *TRAC* loci (see **Fig. 5a**)
307 and administered DARIC-T cells to NSG mice three days post-transfection. This time, no prior *ex*
308 *vivo* expansion and selection was performed before injecting T cells into mice (**Fig. 6a**). No anti-
309 tumor activity was detected in mice treated with DARIC-T cells in the absence of rapamycin,
310 confirming the absence of extracellular receptor dimerization without pharmacological induction
311 (**Fig. 6b,c**). Strikingly, complete tumor control was observed during the first three weeks in all
312 mice treated with rapamycin and DARIC-T cells (**Fig. 6b,c**). While maximal tumor burden was
313 observed in all mice that were not treated with rapamycin three weeks after T cells injection, mice
314 treated with DARIC-T cells in combination with rapamycin survived up to eleven weeks (**Fig.**
315 **6b,c and Supplementary Fig. 8**). Of relevance, we observed a prolonged anti-tumor control in
316 female mice (**Fig. 6b,c and Supplementary Fig. 8**). While the impact of sex as a biological
317 variable warrants further investigation, we note that the female NSG mice weighed less on average
318 (~3-5 grams difference) than their male counterparts at the start of the experiment (see MS source
319 data). Thus, the female mice received both a larger tumor burden and a larger dose of DARIC-T
320 cells. Interestingly, it has recently been reported in a retrospective study of clinical trials for CD19
321 CAR-T cell therapy that the response and survival are significantly superior in female compared
322 to male patients[60]. Altogether, this multiplexed strategy offers the opportunity to use
323 immunosuppressive doses of rapamycin in combination with DARIC-T cells to decrease tumor
324 cell growth and to pharmacologically fine-tune CAR-T cells' activity.
325

326 **DISCUSSION**

327 Engineering primary T cells with programmable nucleases for cell therapy applications remains
328 challenging. In this work, we describe a marker-free selection approach to simultaneously target a
329 therapeutic transgene of interest and a point mutation to the *MTOR* locus to generate dominant
330 cellular resistance to rapamycin. We show that mTORC1 signaling remained functional and cells
331 grew robustly in the presence of rapamycin after targeted transgene integration. Our results further
332 demonstrate that introns provide an additional non-coding location for targeted transgene
333 integration via intron nesting[34,35]. Taking advantage of this naturally occurring genomic
334 architecture allows the co-modification of an endogenous gene during the integration of a

335 therapeutic transgene of interest in a single gene editing event. However, this strategy is limited to
336 moderately active promoters, such as the human *PGK1* promoter used in this study, since
337 transcriptional interference between the overlapping genes[35] would be detrimental for mTORC1
338 signaling, and consequently, CAR-T cell activation and expansion[21,30]. This could be prohibitive
339 for applications where high levels of transgene expression are needed to reach a therapeutic
340 threshold.
341
342 The metabolic competition between cancer and T cells has previously been shown to drive cancer
343 progression[61], and metabolic interventions could be used in combination to improve clinical
344 outcomes[62]. Hence, targeting cancer metabolism via mTORC1 inhibition could potentially slow
345 tumor progression and facilitate complete tumor eradication. Taken together, our findings suggest
346 that rapamycin could be administered to enrich CRISPR-engineered cells *in vivo* while providing
347 a fitness advantage against tumor cells. Of note, since double editing events at two different loci
348 are not statistically independent, rapamycin co-selection could also be performed to enrich a
349 second modification of interest[34,63].
350
351 Our cytotoxicity assays corroborate previous findings regarding the combinatorial impact of
352 rapamycin with *piggyBac*-modified rapamycin-resistant CAR-T cells[27]. Nonetheless, our
353 CRISPR-based strategy offers advantages over the use of a two *piggyBac* transposon vectors
354 system to target a CAR and a large rapamycin-resistant mTOR transgene cassette (≈7.65kb)[27] to
355 random genomic locations[27–29].
356
357 While we focused on the standard $CD19^+$ NALM6 acute lymphoblastic leukemia model during
358 this study, combinatorial CAR-T cell therapy with rapamycin could potentially improve antitumor
359 activity against solid tumors displaying hyperactive mTOR signaling[36,64,65]. One key advantage of
360 our gene targeting approach is the opportunity to use dimerizing agent-regulated immunoreceptor
361 complex (DARIC) switchable between on and off states using rapamycin to develop safer CAR-T
362 cells therapies[31,32,57]. One limitation of the previously reported systems is the use of non-
363 immunosuppressive rapamycin dosing[31] to prevent the inhibition of CAR-T cells' activation,
364 which can be overcome using rapamycin-resistant DARIC-T cells. Our system could be used to
365 fine-tune CAR-T cells activity with rapamycin pulsing to prevent tonic CAR signaling, and

366 consequently, exhaustion[31,66]. In line with this, transient rest induced by a drug-regulatable CAR
367 or the tyrosine kinase inhibitor dasatinib has been shown to restore functionality in exhausted
368 CAR-T cells through epigenetic remodeling[67–69]. Most importantly, rapamycin-regulatable CAR
369 architectures could be used as safety switches to dampen toxicity and severe adverse events
370 associated with cytokine release syndrome[31,67–71].
371
372 During this study, we also identified new rapamycin resistance mutations via saturation prime
373 editing that displayed intermediate levels of mTORC1 signaling in the presence of rapamycin.
374 These additional mutations offer interesting opportunities to investigate the potential of
375 pharmacologically fine-tuning mTORC1 activity for cell therapy applications. mTOR plays key
376 roles in T cell fate decisions and differentiation[30,49]. Reducing mTORC1 signaling has been shown
377 to trigger the formation of stem cell-like memory T cells and also enhance CAR-T cell antitumor
378 activity[50,72]. In addition, it was shown that transient mTOR inhibition with rapamycin rescues 4-
379 1BB CAR-Tregs from tonic signal-induced dysfunction[73]. Considering that mTORC1 signaling
380 acts as a metabolic rheostat[24], fine-tuning this pathway could potentially have a positive impact on
381 CAR-T cells persistence, and consequently, CAR-T cells antitumor activity. While this hypothesis
382 warrants further investigation, our results demonstrate that engineering the *MTOR* locus with
383 CRISPR allows the marker-free selection of cells with different levels of mTORC1 signaling in
384 the presence of rapamycin.
385
386 Altogether, the strategy presented here should facilitate the *ex vivo* and *in vivo* enrichment of
387 CRISPR-engineered cells expressing a therapeutic transgene of interest while offering an
388 opportunity to pharmacologically fine-tune cell signaling, providing a versatile platform for cell
389 therapy applications.
390

391 # METHODS

392 **K562 and NALM6 cell culture and transfection**

393 K562 cells were obtained from the ATCC (CCL-243) and NALM6 cells stably transduced to
394 express a FLUC-T2A-RFP-IRES-Puro reporter gene cassette (Biosettia) were gently provided by
395 Scott McComb (National Research Council of Canada). K562 and NALM6 cells were maintained
396 at 37 °C under 5% CO_2 in RPMI medium supplemented with 10% FBS, penicillin–streptomycin,

397 and GlutaMAX. Cells were routinely tested for the absence of mycoplasma contamination.
398 Rapamycin (Cayman Chemicals, Cat 53123-88-9) was dissolved at 10 mg/ml in DMSO, working
399 dilutions were prepared in water and stored at -20ºC. AZD8055 (STEMCELL Technologies) was
400 dissolved at 10 mM in DMSO, working dilutions were prepared in water and stored at -20ºC.
401 DMSO alone was diluted in water and used as vehicle control. Ouabain octahydrate (Sigma) was
402 dissolved at 5 mg/ml in hot water, working dilutions were prepared in water and stored at -20ºC.
403 K562 and NALM6 cells ($2x10^5$ cells/transfection) were transfected using a Lonza 4D
404 nucleofector™ with a SF nucleofection kit (Lonza) following manufacturer's recommendations.
405 For prime editing transfections, K562 cells were transfected with 0.75 µg of PE vector, 0.25 µg of
406 epegRNA vector, and 0.1 µg of nick sgRNA vector. NALM6 cells were transfected with 50 pmols
407 of SpCas9 RNP (IDT) and 0.75 µg of dsDNA donor harboring *MTOR*-F2108L and a PAM
408 mutation to generate the NALM6-RapaR cell line. Cells were treated with the indicated
409 concentration of rapamycin 3 days post-nucleofection until all non-resistant cells were eliminated.
410

411 **Genome editing vectors and recombinant AAV production**

412 Guide RNAs were designed with CRISPOR[43] and their sequences are provided in the
413 **Supplementary material** section. When required, DNA sequences for the guides were modified
414 at position 1 to encode a G, owing to the transcription requirement of the human U6 promoter.
415 Guide RNAs were cloned into pX330-U6-Chimeric_BB-CBh-hSpCas9 (a gift from Feng Zhang;
416 Addgene 42230) and their sequences are provided in the **Supplementary material** section.
417 Plasmid donors were cloned into pUC19 with short homology arms (700-800 bp) and all sequences
418 were confirmed by Sanger sequencing. Prime editing (PE) experiments were performed with
419 pCMV-PEmax[74] (a gift from David Liu; Addgene 174820), and pU6-tevopreq1-GG-acceptor[41] (a
420 gift from David Liu; Addgene 174038). To repurpose the mTORC1 signaling reporter mVenus-
421 TOSI previously developed for mouse[40], the N-terminal residues (1-82) of the human *PDCD4*
422 gene were codon optimized using the GenSmart™ codon optimization tool, synthesized as a
423 gBlocks™, and cloned into ATP1A1_T804N_hPGK1_mScarlet-I_Donor (Addgene 173207)
424 upstream of the mScarlet-I-NLS cassette using AflII and NcoI. The CD19-CAR-28z-2A-EGFP
425 gene cassette from pSLCAR-CD19-28z (a gift from Scott McComb: Addgene 135991)[54] was
426 cloned into the *MTOR* donor vector by Gibson assembly without the 3xFLAG. The CD19-DARIC
427 expression vector was designed in-house based on previously described constructions[31] and US

428 patent 2012/0266971 A1. The CD22-DARIC construction was designed using a previously
429 described CD22 scFv fragment[59]. DARIC sequences were codon-optimized using GenSmart™
430 codon optimization tool, synthesized by GenScript, and cloned into the AAV6 vector using Gibson
431 assembly. Vectors used for AAV6 production are available at Addgene and their ID are provided
432 in the **Supplementary material** section. The AAV6 vectors were produced by the vector core
433 facility at the Canadian neurophotonics platform (molecular tools). ITR integrity was assessed
434 following BssHII digestion of the AAV plasmid before production. The virus was resuspended in
435 PBS 320 mM NaCl + 5% D-sorbitol + 0.001% pluronic acid (F-68), aliquoted, and stored at −80°C.
436 The vector yields were $1x10^{12}$, $8.5x10^{12}$, and $6.9x10^{12}$ GC/ml for the *MTOR*-F2108L-CD19-CAR-
437 2A-EGFP, *MTOR*-F2108L_CD19_scFv, and TRAC_T2A_CD22-DARIC donors, respectively.
438
439 **Primary human T cells isolation and culture**
440 Primary $CD3^+$ human T cells were isolated from anonymized healthy human donors either from
441 fresh whole blood (WB) or leukocyte reduction system (LRS) chambers (Héma-Québec), or from
442 human peripheral blood leukopaks (STEMCELL). EasySep™ Human T cell isolation kit
443 (STEMCELL) or CD3 microbeads (Miltenyi) were used for positive magnetic selection of $CD3^+$
444 T cells from peripheral blood mononuclear cells (PBMCs). Primary $CD3^+$ T cells were cultured
445 with Immunocult-XF T cell expansion medium supplemented with 1% penicillin-streptomycin and
446 300 U/ml IL-2. Cells were thawed and activated for 3 days with Immunocult™ human
447 CD3/CD28/CD2 T cell activator (STEMCELL) before nucleofection.
448
449 **Primary human T cells transfection**
450 dsDNA donors were produced as described previously[47]. Briefly, donor sequences were cloned
451 into a cloning vector and PCR amplification (25 cycles) was performed using Kapa-HiFi
452 polymerase (Roche). DNA purification was performed by solid-phase reversible immobilization
453 using AMPure XP (Beckman Coulter) magnetic beads. For ribonucleoprotein complex (RNP)
454 formulation, 100 pmols of sgRNAs (Alt-R, IDT) were mixed with 0.8 µl of 100 mg/ml
455 polyglutamic acid (Sigma) and 50 pmols of SpCas9 nuclease (IDT) as previously described[75]. The
456 RNP mix was incubated at 37°C for 10 minutes and the dsDNA donors were added to the mix and
457 incubated at room temperature for 5 minutes before transfection. Primary $CD3^+$ T cells ($1x10^6$
458 cells/transfection) were transfected using a Lonza 4D nucleofector™ (Pulse code EH115) with a

459 P3 nucleofection kit (Lonza) following manufacturer's recommendations with the indicated DNA
460 concentrations. $CD3^+$ T cells were resuspended in 80 µl media without IL-2 directly after
461 nucleofection and incubated at 37°C for 15 minutes before transfer into culture media plates at
462 $1x10^6$ cells/ml. For AAV6 transduction, $CD3^+$ T cells were resuspended in 80 µl media directly
463 after nucleofection and AAV6 vectors were added. Cells were incubated at 37°C for 8 hours at
464 high cell density before transfer into culture media plates. For rapamycin selection, $CD3^+$ T cells
465 were treated with or without 25 nM rapamycin on Day 3 post-nucleofection, restimulated with
466 Immunocult™ human CD3/CD28/CD2 T cell activator (STEMCELL) 4 days post-transfection,
467 and expanded for an additional 7 days.
468
469 **Sanger sequencing analysis and out-out PCRs**
470 Genomic DNA was extracted with QuickExtract DNA extraction solution (EpiCentre) following
471 manufacturer's recommendations. Primers used in this study and the PCR product sizes are
472 provided in the **Supplementary material** section. PCR amplifications were performed with 30
473 cycles of amplification with Phusion polymerase. Sanger sequencing was performed on PCR
474 amplicons to quantify the percentage of edited alleles using TIDE[76], TIDER[77], and BEAT[78]. To
475 quantify the percentage of alleles harboring the *MTOR*-F2108L mutation after targeted transgene
476 integration, we performed PCR amplifications to amplify both WT and HDR alleles with a forward
477 primer binding outside the region of homology of our donors, and a reverse primer binding inside
478 the homology arm upstream of the SpCas9 target sites (out-in PCR). Genomic DNA from WT
479 cells and cells transfected or transduced only with the donor were used as negative controls in all
480 experiments. Kapa-HiFi polymerase was used for out-out PCRs. To detect targeted integration,
481 out-out PCRs were performed with primers that bind outside of the homology regions of the
482 plasmid/dsDNA donors. Wild type K562 or $CD3^+$ T cells genomic DNA was used as a control for
483 all PCRs.
484
485 **Flow cytometry**
486 The percentage of fluorescent cells was quantified using a BD LSRII flow cytometer using
487 FACSdiva v6.1.2 software, and $1x10^5$ cells were analyzed for each condition. For mTORC1
488 signaling assays, cells were washed with PBS and cultured at least 3 days without rapamycin. Cells
489 were treated with the indicated concentration of rapamycin or AZD8055 for 24 hours before

490 analysis. FACS sorting was performed using a BD FACS Aria Fusion flow cytometer for the
491 saturation prime editing experiment, and $5x10^5$ cells were sorted for each condition.
492
493 Multicolor flow cytometry panels were performed using a Cytek Aurora flow cytometer. T cells
494 were stained with fixable viability dye eF506 (Invitrogen Cat 65-0866-18) for 15 minutes at 4°C,
495 then washed and resuspended in Human TruStain FcX blocking solution (BioLegend Cat
496 2711505) and Brilliant Stain Buffer Plus (BD Biosciences Cat 566385) for 10 minutes at room
497 temperature. After blocking, cells were stained with the following antibody cocktail diluted in flow
498 cytometry staining buffer: mouse anti-human CD3 BV750 (BioLegend Cat 344846), mouse anti-
499 human CD4 AF700 (BioLegend Cat 300526), mouse anti-human CD8 PerCP (BioLegend Cat
500 301030), mouse anti-human CD279 BV421 (BioLegend Cat 329920), mouse anti-human CCR7
501 APC-Fire 750 (BioLegend Cat 353246), and mouse anti-human CD45RO PE-Cy7 (Invitrogen Cat
502 25-0457-42). Flow cytometric data were analyzed using SpectroFlo (Cytek) and FlowJo V10 (Tree
503 Star).
504
505 **Saturation prime editing and high-throughput DNA sequencing**
506 The *MTOR*-F2108 saturation epegRNA (tevopreQ1)[41] vector was designed to install NNK codons
507 and a silent R2109R PAM mutation at *MTOR* exon 45, synthesized as a gBlock™ (IDT), and
508 cloned into pU6-tevopreq1-GG-acceptor[41] (a gift from David Liu; Addgene 174038). K562 cells
509 stably expressing the mSc-TOSI reporter were transfected with PE3max-epegRNA (tevopreQ1)
510 vectors and treated with 0.5 μM rapamycin starting 3 days post-transfection until all non-resistant
511 cells were eliminated. Following selection, cells were treated for 24 hours with 0.5 μM rapamycin
512 and FACS-sorted for low mSc-TOSI fluorescence intensity to enrich cells with functional
513 mTORC1 signaling in the presence of rapamycin. Genomic DNA was harvested after selection
514 and after FACS sorting for low and high mSc-TOSI fluorescence intensity. For amplicon
515 sequencing, primers containing Illumina forward and reverse adapters were used for a first round
516 of PCR using the Kapa-HiFi polymerase. PCR products were purified using AMPure XP magnetic
517 beads and their quality was evaluated by electrophoresis. A second round of PCR and bead
518 purification was performed for indexing, and amplicons were sequenced on an Illumina MiSeq
519 instrument. Alignment of amplicon sequences to the reference *MTOR* sequence was performed
520 using CRISPResso2[79], and all possible NNK codons were detected.

521

522 **GUIDE-Seq**

523 GUIDE-Seq was performed as previously described[45,46], except for improvements of the Next
524 Generation Sequencing (NGS) library preparation procedure reported below. GUIDE-Seq oligos
525 harboring 5' phosphorylation modification and two phosphorothioate linkages between the last
526 two nucleotides at the 3' end were synthesized by IDT. Oligos were mixed in 50 mM NaCl, 10
527 mM Tris-HCl (pH 8.0), 1 mM EDTA, and annealed by heating the solution to 95°C for 10 minutes,
528 followed by gradual cooling on a thermocycler. For K562 cells, $2x10^5$ cells were electroporated
529 with 750 ng of SpCas9-sgRNA vectors and 100 pmol of annealed GUIDE-Seq oligos. For primary
530 $CD3^+$ T cells, $1x10^6$ cells were electroporated with 50 pmol SpCas9 RNP and 100 pmol annealed
531 GUIDE-Seq oligos. Genomic DNA was harvested using QIAmp UCP DNA Micro Kit (QIAGEN).
532 GUIDE-Seq oligo tag integration was confirmed using TIDE[76] and DECODR[80] webtools from
533 Sanger sequencing. The library preparation method was improved starting from the original
534 GUIDE-Seq procedure[45,46]. After mechanical fragmentation, end-repair and A-Tailing were
535 directly performed using the NEBNext UltraII DNA kit (New England Biolabs). A new custom
536 universal Y-adapter based on the Illumina TruSeq sequences was designed to include a Unique
537 Molecular Index (UMI) in the sequencing read instead of the index read. This modification enables
538 mixing of GUIDE-Seq libraries with other Illumina library types (amplicon, shotgun, RNASeq,
539 etc.) in the sequencing run by using standard index read lengths. This new adapter was ligated as
540 described in the instructions of the NEBNext UltraII procedure using a final concentration of 133
541 nM. Ligated DNA was purified using 0.9X volume of AMPure XP beads (Beckman-Coulter), then
542 split in 2 for PCR amplifications with either Minus or Plus primers using Q5 DNA Polymerase
543 (New England Biolabs) with the following cycling conditions: 98°C 30 sec; 10 cycles of 98°C 10
544 sec, 55°C 30 sec, 72°C 30 sec; 15 cycles of 98°C 10 sec, 65°C 30 sec, 72°C 30 sec; 72°C 2 min;
545 4°C hold. New primers with Illumina sequence tails were specifically designed for this improved
546 method. The use of Illumina sequences at the Plus/Minus amplification stage eliminates the use of
547 custom primers for sequencing. PCR products were purified with 0.9X AMPure XP beads and
548 quantified using Qubit dsDNA HS Assay (Invitrogen). Then, 10 ng DNA was used for a second
549 PCR amplification with Illumina TruSeq dual-indexing primers (98°C 30 sec; 8 cycles of 98°C 10
550 sec, 55°C 30 sec, 72°C 30 sec; 72°C 2 min; 4°C hold). The barcoding at the PCR stage enables a
551 much simpler and higher multiplexing capacity. PCR products were purified using 0.85X AMPure

552 XP beads, quantified using Qubit dsDNA HS Assay and ran on a Bioanalyzer High Sensitivity
553 DNA chip (Agilent). Samples were pooled in equimolar amounts and sequenced on 1.4% (35M
554 read block) of a NovaSeq S4 PE150 lane (Illumina) at the Centre d'Expertise et de Services
555 Génome Québec (Montréal, QC). The remaining portion of the sequencing lane contained a
556 mixture of library types from multiple organisms (*M. plutonius*, *P. larvae*, *F. graminearum*, *P.*
557 *neglectus*, *Colletotrichum* spp., *Sporothrix* spp.).
558
559 **Analysis of GUIDE-Seq sequencing**
560 A new pipeline, named guideseq_ibis, was designed to analyze the data from the improved
561 GUIDE-Seq procedure (https://github.com/enormandeau/guideseq_ibis). Using this pipeline, the
562 raw reads were trimmed for quality using trimmomatic (v0.36, min_length 100, crop_length 200).
563 Then, only reads containing the expected alien sequence (maximum hamming distance of 1) and
564 only one copy of the ODN sequence (maximum hamming distance of 6) were retained. For these
565 reads, the Unique Read Identifiers (UMIs) and first eight nucleotides were used to rename the
566 sequence. These tagged reads were then mapped onto the latest GRCh38 human genome assembly
567 with bwa (v0.7.17-r1188, -T 10) and then samtools (v1.12, -S -q 1 -F 4 -F 256 -F 2048). The
568 alignment sam files were then sorted by chromosome name and position. The UMI and eight first
569 nucleotides of the reads and the starting positions of their alignments were used to detect duplicated
570 reads. Namely, only one copy of reads with identical UMIs, eight first nucleotides, and alignment
571 start position were kept. Then, Double Stranded Breaks (DSBs) were identified. For this, alignment
572 sites were scanned for peaks of coverage in decreasing order of depth of coverage and pairs of
573 ODN+ and ODN- were reported until the pairs did not meet the minimum coverage threshold
574 (min_length 100, min_coverage 50, window_size 10, position_error 5, bin_size 10000). To
575 account for small errors in sequencing and mapping, read counts are collected within
576 `window_size` nucleotides around each peak and pairs of ODN sequences were kept if they fell
577 withing `position_error` nucleotides of their relative expected positions. Identified sequences on
578 target and off-target were reported for each sample with their chromosome and position
579 localisation, the identifier and name of any gene they overlapped (using a simplifited annotation
580 table from GRCh38.p14), and metrics about the counts of the ODN+ and ODN- reads. Finally,
581 annotation of the found targets and off-targets was performed to add information about the guide's
582 name, the distance between the target sequence and the expected guide sequence, as well as a

583 representation of the modified nucleotides along the guide sequence. The chromosomal positions
584 and the targeted gene (were applicable) of all off-targets are provided in the **Supplementary**
585 **material** section.
586
587 **Cytotoxicity assays**
588 Luciferase-based cytotoxic assays were performed as previously described[10,81]. After rapamycin
589 selection, CD19-CAR-T cells were washed with PBS, and co-cultured in 96-well plates in
590 supplemented RPMI medium with NALM6 cells stably expressing firefly luciferase and RFP at
591 the indicated effector to target ratio (E:T) for 18 hours. Target cells incubated with WT $CD3^+$ T
592 cells were used to determine maximal luciferase expression (maximal relative light units; RLU_{max}).
593 After coculture, an equal volume of luciferase substrate (Bright-Glo, Promega) was added to each
594 well. Emitted light was detected with a Tecan luminescence plate reader and cell lysis was
595 determined as $(1 – (RLU_{sample})/(RLU_{max})) \times 100$. FACS-based cytotoxicity assays were performed
596 as previously described[31], except with a prolonged coculture time. T cells were washed with PBS,
597 and cocultured in 12-well plates in supplemented RPMI medium with 50:50 mixtures of
598 rapamycin-resistant K562-EBFP (CD19-negative) cells and NALM6-RFP cells at the indicated
599 effector to target ratio (E:T) for 72 hours. Cell viability was assessed using the fixable viability
600 dye eFluor™ 660 (eBioscience). The ratio of viable NALM6-RFP and K562-EBFP cells following
601 coculture in the presence or absence of 25 nM rapamycin was used to calculate the percentage of
602 cytotoxicity. Target cells incubated with WT $CD3^+$ T cells were used to determine maximal
603 NALM6-RFP growth.
604
605 **Mouse systemic tumor model.**
606 The *in vivo* CAR-T cells experiments were performed according to the *Canadian Guide for the*
607 *Care and Use of Laboratory Animals*. The Université Laval Animal Care and Use Committee
608 approved the procedure. 8-10 weeks-old NOD/SCID/IL-2Rγ-null (NSG) male and female mice
609 were acquired from Jackson Laboratory. 0.5×10^6 NALM6-RFP-FLUC cells were administered
610 via tail vein injection. Three days later, daily rapamycin treatment (4 mg/kg) or vehicle (filter-
611 sterilized solution of 5% Tween80, 5% PEG-400, 0.7% DMSO) was administered by
612 intraperitoneal (IP) injection. Four days after tumor inoculation, 2×10^6 CAR-T cells (≈86% CAR-
613 2A-$EGFP^+$ cells) or untransduced (UT) T cells were administered via tail vein injection. CAR-T

614 cells expanded for 14 days, including 8 days of treatment/selection with 25 nM rapamycin, were
615 used for the *in vivo* experiment. The same protocol was used for the multiplexed DARIC-T cells
616 experiment, but DARIC-T cells were administered three days post-transfection without *ex vivo*
617 expansion/selection. Tumor burden was measured twice per week by bioluminescence imaging
618 using the IVIS LuminaIII Imaging System (PerkinElmer). Mice were anesthetized using
619 isoflurane, and 150 mg/kg D-Luciferin (Goldbio) was administered via IP injection. Data were
620 analyzed using the Living Image software (PerkinElmer). The maximum tumor burden and
621 survival endpoint were defined by hindlimb paralysis or other clinical signs of distress. There were
622 no instances in which this maximum tumor burden was exceeded.
623

624 **DATA AVAILABILITY**

625 Source data for the figures are provided as a Source Data file. All raw Sanger sequencing data
626 generated in this study are available on request from the corresponding author [YD].
627

628 **CODE AVAILABILITY**

629 The adapted GUIDE-Seq analysis pipeline developed and used in this study is freely available at
630 https://github.com/enormandeau/guideseq_ibis.
631

632 **REFERENCES**

633 1. Brentjens, R. J. *et al.* CD19-targeted t cells rapidly induce molecular remissions in adults
634 with chemotherapy refractory acute leukemia. *Sci. Transl. Med.* **5**, 177ra38 (2013).
635 2. Lee, D. W. *et al.* T cells expressing CD19 chimeric antigen receptors for acute
636 lymphoblastic leukaemia in children and young adults: A phase 1 dose-escalation trial.
637 *Lancet* **385**, 517–528 (2015).
638 3. Neelapu, S. S. *et al.* Axicabtagene ciloleucel CAR T-cell therapy in refractory large B-
639 Cell lymphoma. *N. Engl. J. Med.* **377**, 2531–2544 (2017).
640 4. Park, J. H. *et al.* Long-term follow-up of CD19 CAR therapy in acute lymphoblastic
641 leukemia. *N. Engl. J. Med.* **378**, 449–459 (2018).
642 5. Maloney, D. G. Anti-CD19 CAR T cell therapy for lymphoma — off to the races! *Nat.*
643 *Rev. Clin. Oncol.* **16**, 279–280 (2019).
644 6. Labanieh, L., Majzner, R. G. & Mackall, C. L. Programming CAR-T cells to kill cancer.

645 *Nat. Biomed. Eng.* **2**, 377–391 (2018).
646 7. Larson, R. C. & Maus, M. V. Recent advances and discoveries in the mechanisms and
647 functions of CAR T cells. *Nat. Rev. Cancer* **21**, 145–161 (2021).
648 8. Bailey, S. R. & Maus, M. V. Gene editing for immune cell therapies. *Nat. Biotechnol.* **37**,
649 1425–1434 (2019).
650 9. Ellis, G. I., Sheppard, N. C. & Riley, J. L. Genetic engineering of T cells for
651 immunotherapy. *Nat. Rev. Genet.* **16**, 103–107 (2021).
652 10. Eyquem, J. *et al.* Targeting a CAR to the TRAC locus with CRISPR/Cas9 enhances
653 tumour rejection. *Nature* **543**, 113–117 (2017).
654 11. Mansilla-soto, J. *et al.* HLA-independent T cell receptors for targeting tumors with low
655 antigen density. *Nat. Med.* **28**, 345–352 (2022).
656 12. Wei, J. *et al.* Targeting REGNASE-1 programs long-lived effector T cells for cancer
657 therapy. *Nature* **576**, 471–476 (2019).
658 13. Giuffrida, L. *et al.* CRISPR/Cas9 mediated deletion of the adenosine A2A receptor
659 enhances CAR T cell efficacy. *Nat. Commun.* **12**, 3236 (2021).
660 14. Carnevale, J. *et al.* RASA2 ablation in T cells boosts antigen sensitivity and long-term
661 function. *Nature* **609**, 174–182 (2022).
662 15. Depil, S., Duchateau, P., Grupp, S. A., Mufti, G. & Poirot, L. 'Off-the-shelf' allogeneic
663 CAR T cells: development and challenges. *Nat. Rev. Drug Discov.* **19**, 185–199 (2020).
664 16. Stadtmauer, E. A. *et al.* CRISPR-engineered T cells in patients with refractory cancer.
665 *Science* **7365**, eaba7365 (2020).
666 17. Ottaviano, G. *et al.* Phase 1 clinical trial of CRISPR-engineered CAR19 universal T cells
667 for treatment of children with refractory B cell leukemia. *Sci. Transl. Med.* **3010**,
668 eabq3010 (2022).
669 18. Shy, B. R. *et al.* High-yield genome engineering in primary cells using a hybrid ssDNA
670 repair template and small-molecule cocktails. *Nat. Biotechnol.* (2022)
671 doi:10.1038/s41587-022-01418-8.
672 19. Paul, B. *et al.* Efficient enrichment of gene-modified primary T cells via CCR5-Targeted
673 integration of mutant dihydrofolate reductase. *Mol. Ther. Methods Clin. Dev.* **9**, 347–357
674 (2018).
675 20. Wiebking, V. *et al.* Metabolic engineering generates a transgene-free safety for cell

676 therapy. *Nat. Biotechnol.* **38**, 1441–1450 (2020).
677 21. Saxton, R. A. & Sabatini, D. M. mTOR signaling in growth, metabolism, and disease. *Cell*
678 **168**, 960–976 (2017).
679 22. Battaglioni, S., Benjamin, D., Wälchli, M., Maier, T. & Hall, M. N. mTOR substrate
680 phosphorylation in growth control. *Cell* **185**, 1814–1836 (2022).
681 23. Liu, G. Y. & Sabatini, D. M. mTOR at the nexus of nutrition, growth, ageing and disease.
682 *Nat. Rev. Mol. Cell Biol.* **21**, 183–203 (2020).
683 24. Valvezan, A. J. & Manning, B. D. Molecular logic of mTORC1 signalling as a metabolic
684 rheostat. *Nat. Metab.* **1**, 321–333 (2019).
685 25. Mossmann, D., Park, S. & Hall, M. N. mTOR signalling and cellular metabolism are
686 mutual determinants in cancer. *Nat. Rev. Cancer* **18**, 744–757 (2018).
687 26. Sun, Q. *et al.* Mammalian target of rapamycin up-regulation of pyruvate kinase isoenzyme
688 type M2 is critical for aerobic glycolysis and tumor growth. *Proc. Natl. Acad. Sci. U. S. A.*
689 **108**, 4129–4134 (2011).
690 27. Huye, L. E. *et al.* Combining mTor inhibitors with rapamycin-resistant T cells: A two-
691 pronged approach to tumor elimination. *Mol. Ther.* **19**, 2239–2248 (2011).
692 28. Micklethwaite, K. P. *et al.* Investigation of product-derived lymphoma following infusion
693 of piggyBac-modified CD19 chimeric antigen receptor T cells. *Blood* **138**, 1391–1405
694 (2021).
695 29. Bishop, D. C. *et al.* Development of CAR T-cell lymphoma in 2 of 10 patients effectively
696 treated with piggyBac-modified CD19 CAR T cells. *Blood* **138**, 1504–1509 (2021).
697 30. Chi, H. Regulation and function of mTOR signalling in T cell fate decisions. *Nat. Rev.*
698 *Immunol.* **12**, 325–338 (2012).
699 31. Leung, W.-H. *et al.* Sensitive and adaptable pharmacological control of CAR T cells
700 through extracellular receptor dimerization. *JCI Insight* **4**, e124430 (2019).
701 32. Wu, C. Y., Roybal, K. T., Puchner, E. M., Onuffer, J. & Lim, W. A. Remote control of
702 therapeutic T cells through a small molecule-gated chimeric receptor. *Science* **350**,
703 aab4077 (2015).
704 33. Erwood, S. *et al.* Saturation variant interpretation using CRISPR prime editing. *Nat.*
705 *Biotechnol.* **40**, 885–895 (2022).
706 34. Levesque, S. *et al.* Marker-free co-selection for successive rounds of prime editing in

707 human cells. *Nat. Commun.* **13**, 5909 (2022).
708 35. Wright, B. W., Molloy, M. P. & Jaschke, P. R. Overlapping genes in natural and
709 engineered genomes. *Nat. Rev. Genet.* **23**, 154–168 (2021).
710 36. Wagle, N. *et al.* Response and acquired resistance to everolimus in anaplastic thyroid
711 cancer. *N. Engl. J. Med.* **371**, 1426–1433 (2014).
712 37. Lorenz, M. C. & Heitman, J. TOR mutations confer rapamycin resistance by preventing
713 interaction with FKBP12-rapamycin. *J. Biol. Chem.* **270**, 27531–27537 (1995).
714 38. Rodrik-Outmezguine, V. S. *et al.* Overcoming mTOR resistance mutations with a new-
715 generation mTOR inhibitor. *Nature* **534**, 272–276 (2016).
716 39. Choi, J., Chen, J., Schreiber, S. L. & Clardy, J. Structure of the FKBP12-rapamycin
717 complex interacting with the binding domain of human FRAP. *Science* **273**, 239–242
718 (1996).
719 40. Oki, T. *et al.* Imaging dynamic mTORC1 pathway activity in vivo reveals marked shifts
720 that support time-specific inhibitor therapy in AML. *Nat. Commun.* **12**, 245 (2021).
721 41. Nelson, J. W. *et al.* Engineered pegRNAs improve prime editing efficiency. *Nat.*
722 *Biotechnol.* **40**, 402–410 (2021).
723 42. Chresta, C. M. *et al.* AZD8055 is a potent, selective, and orally bioavailable ATP-
724 competitive mammalian target of rapamycin kinase inhibitor with in vitro and in vivo
725 antitumor activity. *Cancer Res.* **70**, 288–298 (2010).
726 43. Concordet, J. P. & Haeussler, M. CRISPOR: Intuitive guide selection for CRISPR/Cas9
727 genome editing experiments and screens. *Nucleic Acids Res.* **46**, 242–245 (2018).
728 44. Vakulskas, C. A. *et al.* A high-fidelity Cas9 mutant delivered as a ribonucleoprotein
729 complex enables efficient gene editing in human hematopoietic stem and progenitor cells.
730 *Nat. Med.* **24**, 1216–1224 (2018).
731 45. Tsai, S. Q. *et al.* GUIDE-seq enables genome-wide profiling of off-target cleavage by
732 CRISPR-Cas nucleases. *Nat. Biotechnol.* **33**, 187–198 (2015).
733 46. Malinin, N. L. *et al.* Defining genome-wide CRISPR–Cas genome-editing nuclease
734 activity with GUIDE-seq. *Nat. Protoc.* **16**, 5592–5615 (2021).
735 47. Roth, T. L. *et al.* Reprogramming human T cell function and specificity with non-viral
736 genome targeting. *Nature* **559**, 405–409 (2018).
737 48. Mahalati, K. & Kahan, B. D. Clinical pharmacokinetics of sirolimus. *Clin.*

738 *Pharmacokinet.* **40**, 573–585 (2001).
739 49. Araki, K. *et al.* mTOR regulates memory CD8 T-cell differentiation. *Nature* **460**, 108–112
740 (2009).
741 50. Dormond, O., Romero, P., Zhang, L. & Romero, P. Modulation of mTOR signalling
742 triggers the formation of stem cell-like memory T cells. *EBioMedicine* **4**, 50–61 (2016).
743 51. Long, A. H. *et al.* 4-1BB costimulation ameliorates T cell exhaustion induced by tonic
744 signaling of chimeric antigen receptors. *Nat. Med.* **21**, 581–590 (2015).
745 52. Philipson, B. I. *et al.* 4-1BB costimulation promotes CAR T cell survival through
746 noncanonical NF-kB signaling. *Sci. Signal.* **13**, eaay8248 (2020).
747 53. Cappell, K. M. & Kochenderfer, J. N. A comparison of chimeric antigen receptors
748 containing CD28 versus 4-1BB costimulatory domains. *Nat. Rev. Clin. Oncol.* **18**, 715–
749 727 (2021).
750 54. Bloemberg, D. *et al.* A high-throughput method for characterizing novel chimeric antigen
751 receptors in Jurkat cells. *Mol. Ther. - Methods Clin. Dev.* **16**, 238–254 (2020).
752 55. Muller, Y. D. *et al.* The CD28-transmembrane domain mediates chimeric antigen receptor
753 heterodimerization with CD28. *Front. Immunol.* **12**, 639818 (2021).
754 56. Majzner, R. G. & Mackall, C. L. Clinical lessons learned from the first leg of the CAR T
755 cell journey. *Nat. Med.* **25**, 1341–1355 (2019).
756 57. Flugel, C. L. *et al.* Overcoming on-target, off-tumour toxicity of CAR T cell therapy for
757 solid tumours. *Nat. Rev. Clin. Oncol.* **20**, 49–62 (2023).
758 58. Shah, N. N. & Fry, T. J. Mechanisms of resistance to CAR T cell therapy. *Nat. Rev. Clin.*
759 *Oncol.* **16**, 372–385 (2019).
760 59. Fry, T. J. *et al.* CD22-targeted CAR T cells induce remission in B-ALL that is naive or
761 resistant to CD19-targeted CAR immunotherapy. *Nat. Med.* **24**, 20–28 (2018).
762 60. Buecklein, V. L. *et al.* Impact of sex on clinical outcomes after CD19 CAR T-cell therapy
763 for large B-cell lymphoma: Response and survival are significantly superior in female
764 compared to male patients. *Blood* **142**, 3787 (2023).
765 61. Chang, C. H. *et al.* Metabolic competition in the tumor microenvironment is a driver of
766 cancer progression. *Cell* **162**, 1229–1241 (2015).
767 62. McGuirk, S., Audet-Delage, Y. & St-Pierre, J. Metabolic fitness and plasticity in cancer
768 progression. *Trends in Cancer* **6**, 49–61 (2020).

769 63. Agudelo, D. *et al.* Marker-free coselection for CRISPR-driven genome editing in human
770 cells. *Nat. Methods* **14**, 615–620 (2017).
771 64. Grabiner, B. C. *et al.* A diverse array of cancer-associated MTOR mutations are
772 hyperactivating and can predict rapamycin sensitivity. *Cancer Discov.* **4**, 554–563 (2014).
773 65. Wagle, N. *et al.* Activating mTOR mutations in a patient with an extraordinary response
774 on a phase I trial of everolimus and pazopanib. *Cancer Discov.* **4**, 546–553 (2014).
775 66. Gumber, D. & Wang, L. D. Improving CAR-T immunotherapy: Overcoming the
776 challenges of T cell exhaustion. *eBioMedicine* **77**, 103941 (2022).
777 67. Mestermann, K. *et al.* The tyrosine kinase inhibitor dasatinib acts as a pharmacologic
778 on/off switch for CAR T cells. *Sci. Transl. Med.* **11**, eaau5907 (2019).
779 68. Weber, E. W. *et al.* Pharmacologic control of CAR-T cell function using dasatinib. *Blood*
780 *Adv.* **3**, 711–717 (2019).
781 69. Weber, E. W. *et al.* Transient rest restores functionality in exhausted CAR-T cells through
782 epigenetic remodeling. *Science* **372**, eaba1786 (2021).
783 70. Fajgenbaum, D. C. & June, C. H. Cytokine storm. *N. Engl. J. Med.* **383**, 2255–2273
784 (2020).
785 71. Morris, E. C., Neelapu, S. S., Giavridis, T. & Sadelain, M. Cytokine release syndrome and
786 associated neurotoxicity in cancer immunotherapy. *Nat. Rev. Immunol.* **22**, 85–96 (2022).
787 72. Alizadeh, D. *et al.* IL15 enhances CAR-T cell antitumor activity by reducing mTORC1
788 activity and preserving their stem cell memory phenotype. *Cancer Immunol. Res.* **7**, 759–
789 772 (2019).
790 73. Lamarthée, B. *et al.* Transient mTOR inhibition rescues 4-1BB CAR-Tregs from tonic
791 signal-induced dysfunction. *Nat. Commun.* **12**, 6446 (2021).
792 74. Chen, P. J. *et al.* Enhanced prime editing systems by manipulating cellular determinants of
793 editing outcomes. *Cell* **184**, 5635–5652 (2021).
794 75. Nguyen, D. N. *et al.* Polymer-stabilized Cas9 nanoparticles and modified repair templates
795 increase genome editing efficiency. *Nat. Biotechnol.* **38**, 44.49 (2019).
796 76. Brinkman, E. K., Chen, T., Amendola, M. & Van Steensel, B. Easy quantitative
797 assessment of genome editing by sequence trace decomposition. *Nucleic Acids Res.* **42**,
798 e168 (2014).
799 77. Brinkman, E. K. *et al.* Easy quantification of template-directed CRISPR/Cas9 editing.

800 *Nucleic Acids Res.* **46**, e58 (2018).
801 78. Xu, L., Liu, Y. & Han, R. BEAT: A Python program to quantify base editing from Sanger
802 sequencing. *Cris. J.* **2**, 223–229 (2019).
803 79. Clement, K. *et al.* CRISPResso2 provides accurate and rapid genome editing sequence
804 analysis. *Nat. Biotechnol.* **37**, 215–226 (2019).
805 80. Bloh, K. *et al.* Deconvolution of complex DNA repair (DECODR): establishing a novel
806 deconvolution algorithm for comprehensive analysis of CRISPR-edited Sanger
807 sequencing data. *Cris. J.* **4**, 120–131 (2021).
808 81. Hamieh, M. *et al.* CAR T cell trogocytosis and cooperative killing regulate tumour antigen
809 escape. *Nature* **568**, 112–116 (2019).
810

811 **ACKNOWLEDGEMENTS**

812 This study was supported by a grant from Mitacs and by the Fondation du CHU de Québec. JJ. L.
813 is supported by a CIHR Project Grant (PJT407274). BC Cancer Foundation funded B.H.N. S.L.
814 was supported by a Frederick Banting and Charles Best Canada graduate scholarship from CIHR,
815 and a Graduate student scholarship from the Fonds de la Recherche du Québec-Santé (FRQS).
816 G.C. holds a Vanier Canada graduate scholarship from CIHR. Salary support was provided by the
817 FRQS to Y.D. B.B. and G.M. are supported by the "Programme d'appui aux plateformes
818 technologiques stratégiques" from the Ministère de l'Économie, de l'Innovation et de l'Énergie
819 Québec. We thank the staff at the flow cytometry core facility of the CHU de Quebec Research
820 Center for their training and assistance. We thank Marie-Ève Paquet and the vector core facility
821 staff at the Canadian neurophotonics platform for AAV6 production. We also thank Scott
822 McComb (National Research Council) for kindly providing NALM6-RFP-FLUC cells.
823

824 **COMPETING INTERESTS**

825 S.L. and Y.D. are co-inventors on a patent application (WO 2023/015376 A1) related to this work.
826

827 **AUTHOR'S CONTRIBUTIONS**

828 Conceptualization, S.L. and Y.D.; methodology, S.L., G.C., V.D., C.G., JP. F., S.V., E.N., G.M.,
829 N.D., J.L., B.B., JJ. L., and Y.D.; investigation, S.L., G.C., V.D., C.G., JP. F., S.V., E.N., G.M.,
830 N.D., J.L., B.B., JJ. L., and Y.D.; writing original draft, S.L.; writing, review and editing, S.L.,

and Y.D.; supervision, J.L., B.B., JJ. L., and Y.D.; funding acquisition, J.L., JJ. L., and Y.D. All authors reviewed the manuscript and approved its final version.

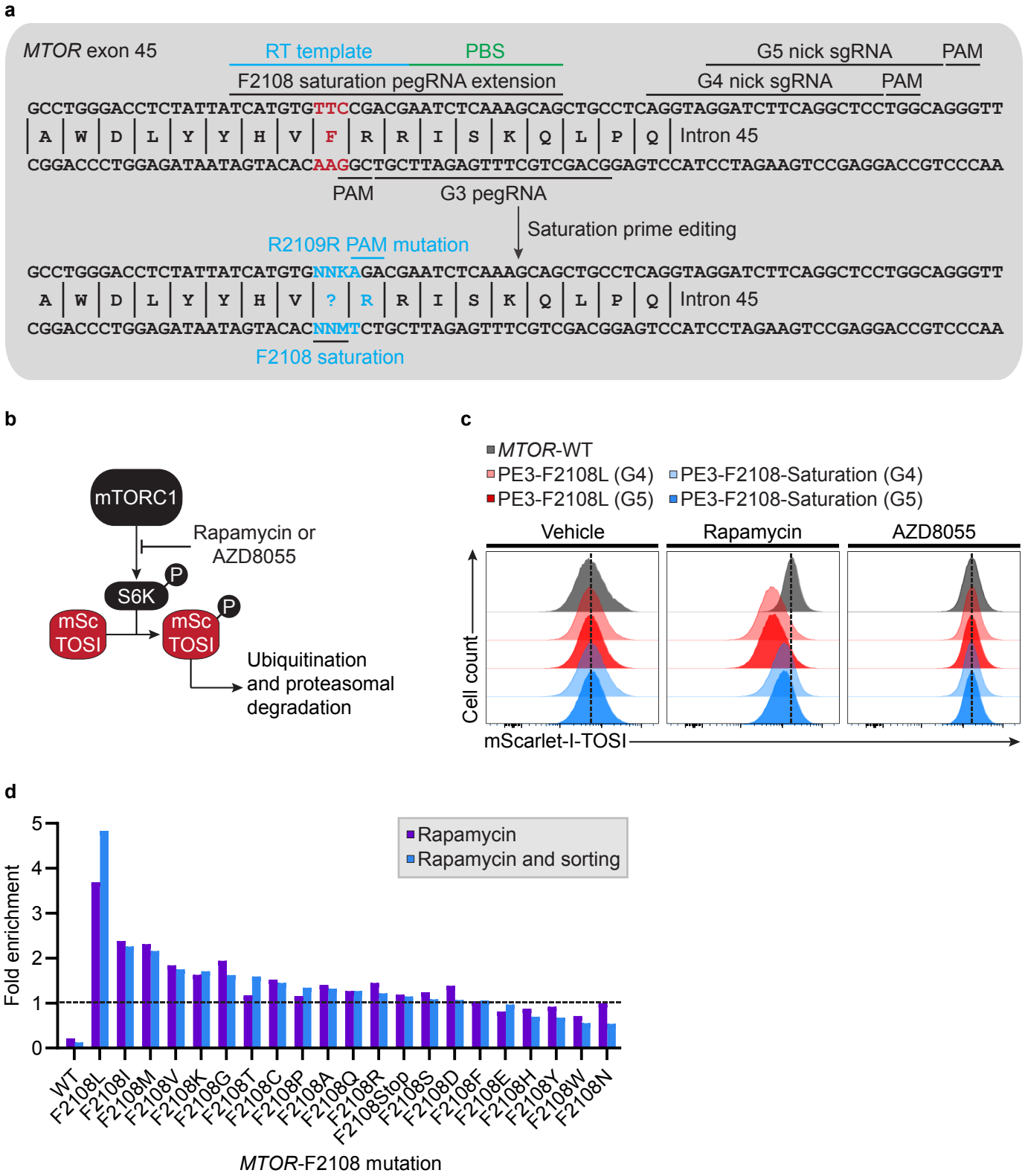

Figure 1
Levesque et al.

832 **Figure 1. Identification of mutations conferring rapamycin resistance via saturation prime**
833 **editing.** (**a**) Schematic representation of the SpCas9 target sites, the reverse transcriptase (RT)
834 template and the primer binding site (PBS) used to perform genome editing at *MTOR*. To perform
835 saturation prime editing, G3 is used as a pegRNA, and G4 or G5 are used as a complementary nick
836 sgRNA (PE3). The *MTOR*-F2108 codon is mutated to NNK and an additional silent PAM mutation
837 is introduced. (**b**) Schematic of mScarlet-I mTOR signaling indicator (mSc-TOSI) degradation
838 under mTORC1 signaling. (**c**) Histogram plot of mSc-TOSI intensity in bulk populations of cells
839 harboring different *MTOR*-F2108 mutations. Where indicated, cells were treated for 24 hours with
840 50 nM rapamycin or 50 nM AZD8055 before FACS analysis. Representative images are from one
841 of two independent biological replicates performed at different times with equivalent results. (**d**)
842 High throughput sequencing quantification of the *MTOR*-F2108 mutations introduced via
843 saturation prime editing following rapamycin selection and FACS sorting. The fold enrichment of
844 each *MTOR*-F2108 mutation was calculated from the before selection sample.

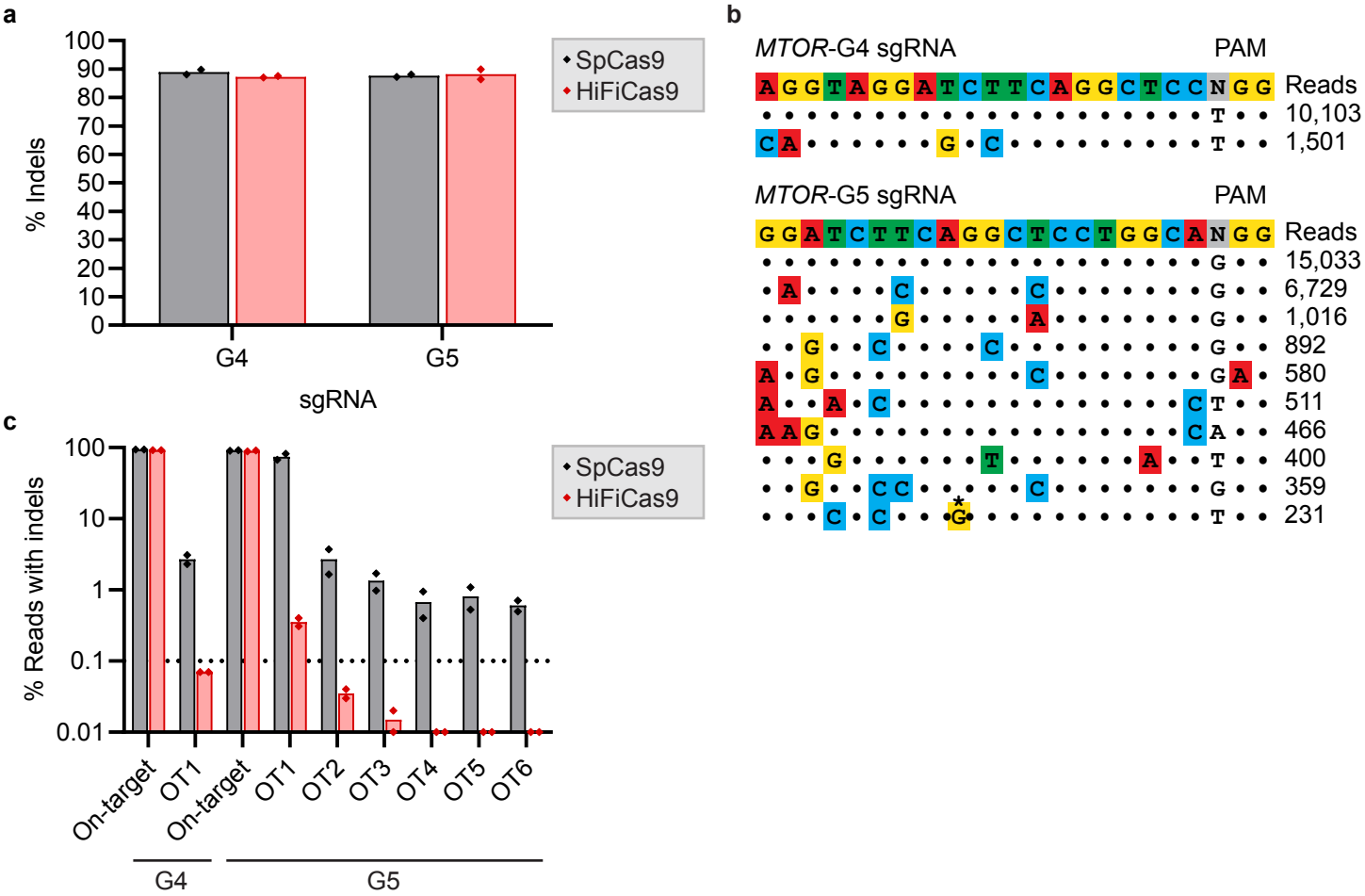

Figure 2
Levesque et al.

845 **Figure 2. Identification of highly active and specific sgRNAs targeting the *MTOR* locus.** (**a**)
846 Small indels quantification as determined by TIDE analysis from Sanger sequencing. Primary
847 $CD3^+$ and $CD8^+$ T cells were transfected with the indicated nuclease/sgRNA RNPs and genomic
848 DNA was harvested 3 days post-transfection. $n = 2$ independent biological replicates performed at
849 different times with $CD3^+$ and $CD8^+$ T cells from two different healthy donors. (**b**) Candidate off-
850 target sites identified using GUIDE-Seq. $CD3^+$ T cells were transfected with SpCas9 RNPs
851 targeting *MTOR* intron 45 and GUIDE-Seq dsDNA. Four days post-nucleofection, $CD3^+$ T cells
852 were restimulated and expanded for an additional 7 days. Genomic DNA was harvested after
853 expansion (11 days post-nucleofection). Dots represent matches with the intended target sequence,
854 mismatches are colored, and nucleotide bulges are highlighted with a star. GUIDE-Seq read counts
855 are from one of two independent biological replicates performed with $CD3^+$ T cells from two
856 different donors (see **Supplementary Fig. 3**). (**c**) Small indels quantification as determined by
857 CRISPResso2 analysis from amplicon sequencing. Primary $CD3^+$ T cells were transfected with
858 the indicated nuclease/sgRNA RNPs and genomic DNA was harvested 3 days post-transfection. n
859 $= 2$ independent biological replicates performed with $CD3^+$ T cells from two different donors.

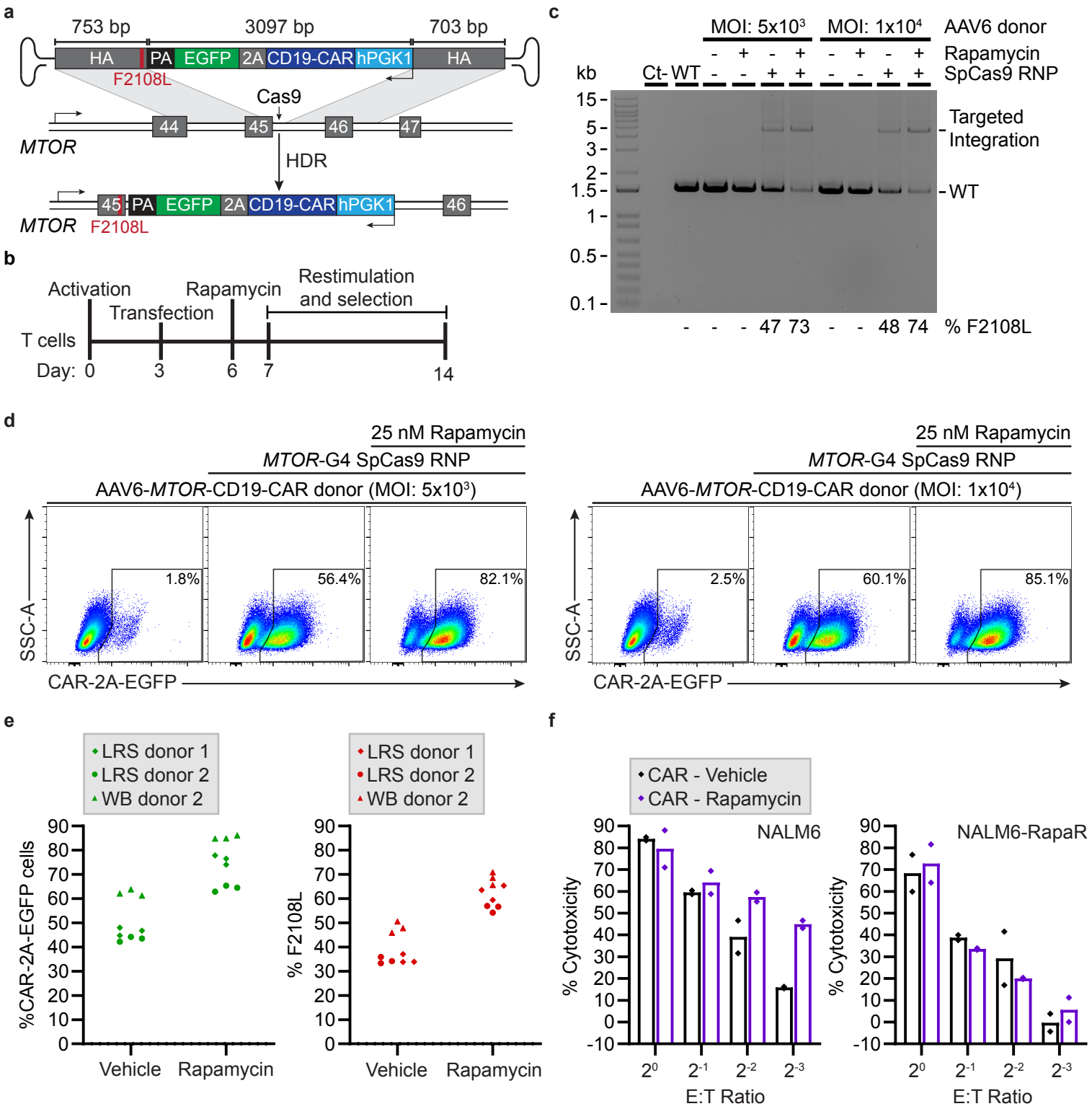

Figure 3
Levesque et al.

860 **Figure 3. Targeting a CAR to the *MTOR* locus allows the enrichment of rapamycin-resistant**
861 **CAR-T cells.** (**a**) Schematic representation of CD19-CAR-2A-EGFP targeting to the reverse DNA
862 strand of the *MTOR* locus using an AAV6 donor. The F2108L mutation is introduced via the left
863 homology arm (HA) and transgene expression is driven by a human *PGK1* promoter. (**b**)
864 Representative timeline for nucleofection and *ex vivo* rapamycin selection. (**c**) Out-Out PCR for
865 CD19-CAR-2A-EGFP knock-in detection at *MTOR*. Whole blood (WB) primary $CD3^+$ T cells
866 from WB donor 1 (WB 1) were transfected with a SpCas9-G4 RNP and transduced with an AAV6
867 vector with the indicated multiplicity of infection (MOI). T cells were treated (rapamycin) or not
868 (vehicle) with 25 nM rapamycin 3 days post-transfection for 8 days. The percentage of edited
869 alleles was determined by TIDER from Sanger sequencing. $n = 1$ experiment. (**d**) Same as in (**c**),
870 but FACS-based quantification of targeted CD19-CAR-2A-EGFP integration. (**e**) Same as in (**c,d**)
871 with a MOI of $5x10^3$ and primary $CD3^+$ T cells isolated from WB or a leukocyte reduction system
872 (LRS) from three additional healthy donors. $n = 3$ independent biological replicates performed in
873 triplicate at different times with $CD3^+$ T cells from the indicated healthy donor. Each data point
874 represents a technical replicate. (**e**) Luciferase-based cytotoxicity assay. Following rapamycin
875 selection, CD19-CAR-T cells were incubated with the indicated effector to target (E:T) ratio with
876 NALM6 cells stably expressing firefly luciferase (FLUC) and 25 nM rapamycin. Rapamycin-
877 resistant NALM6 cells harboring the *MTOR*-F2108L mutation (NALM6-RapaR) were used as a
878 control to analyze the combinatorial impact of rapamycin. Luminescence was measured after 18
879 hours of incubation. $n = 2$ independent biological replicates performed at different times with $CD3^+$
880 T cells from two different healthy donors (WB donor 1 and LRS donor 2). Each data point
881 represents the average of three technical replicates. *hPGK1*, human phosphoglycerate kinase 1
882 promoter. PA, polyadenylation signal. HA, homology arm.
883

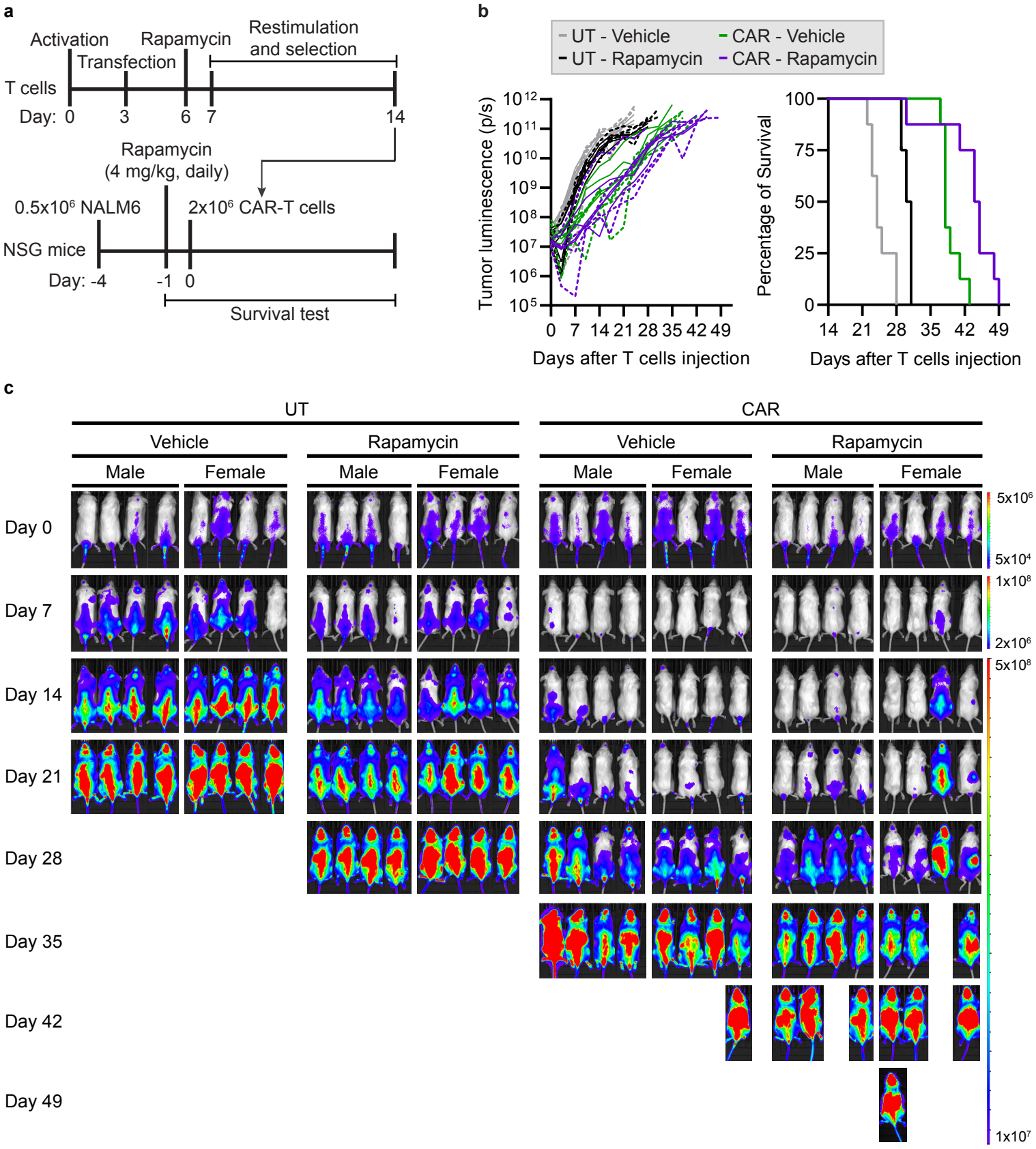

Figure 4
Levesque et al.

884 **Figure 4. Combinatorial CAR-T cell therapy with rapamycin slows leukemia progression *in***
885 ***vivo*.** (**a**) Timeline and experimental setup for the pre-B acute lymphoblastic leukemia xenograft
886 mouse model. Male and female NSG mice were challenged with 0.5 x 10^5 NALM6-RFP-FLUC
887 cells and daily rapamycin treatment (4 mg/kg) started three days later. Four days after tumor
888 inoculation, 2 x 10^6 untransduced (UT) T cells or CD19-CAR-T cells were injected (Donor ID
889 WB2, see **Fig. 3e**). (**b**) Bioluminescence (BLI) quantification and Kaplan-Meier survival plot.
890 Leukemia engraftment, bio-distribution, and tumor progression were assessed by BLI imaging two
891 times per week. The radiance (photons/s) of the regions of interest (ROIs) corresponds to the area
892 containing the whole back side of the body. Radiance quantifications are illustrated with full and
893 dotted lines for male and female mice, respectively. n = 8 mice per group. (**c**) BLI and tumor bio-
894 distribution of all mice from (**b**) over seven weeks. The color barcode represents the radiance scale
895 (photons/s/cm^2/sr).

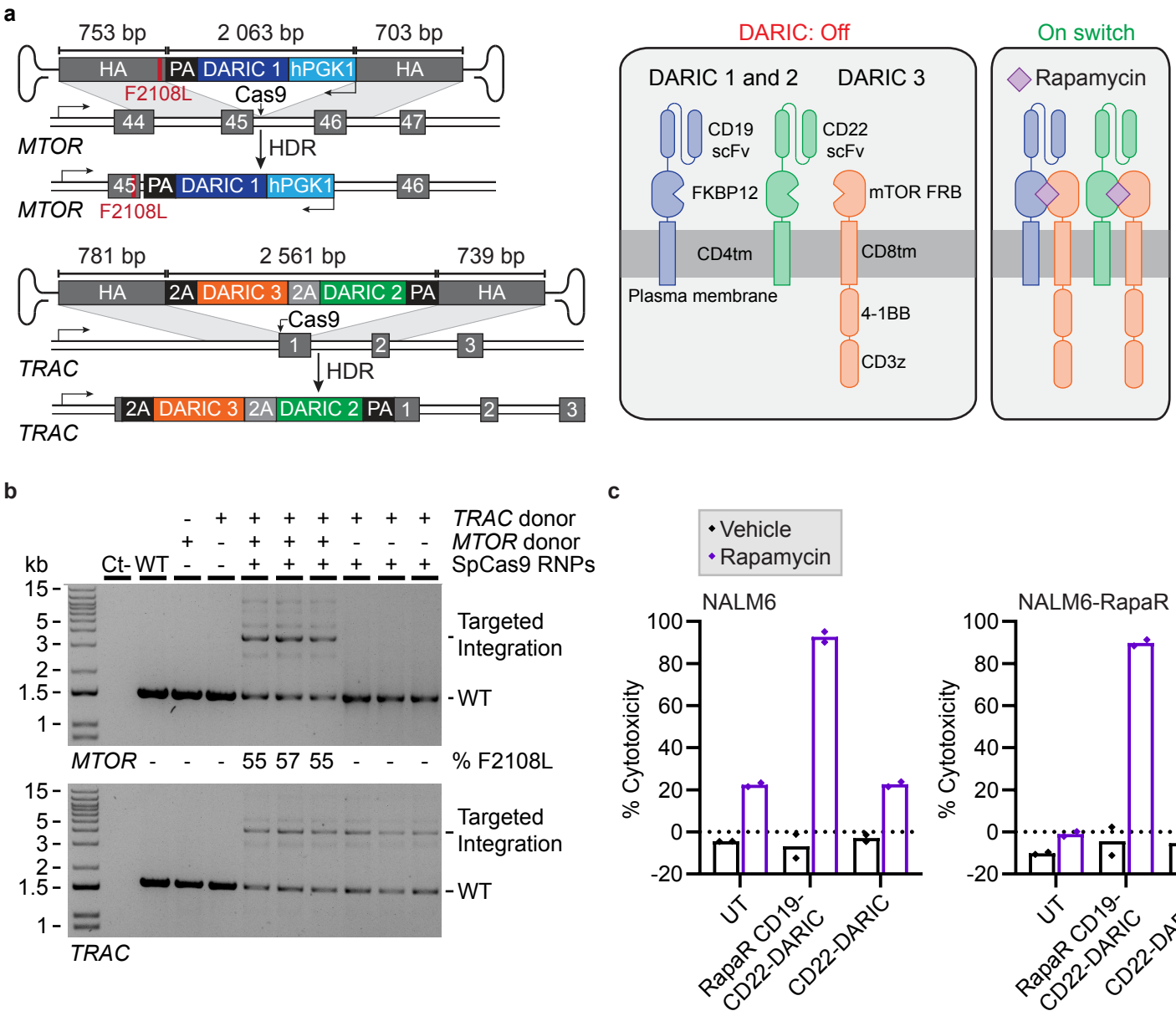

Figure 5
Levesque et al.

896 **Figure 5. Multiplexed DARIC targeting to the *MTOR* and *TRAC* loci allows pharmacological**
897 **control of CAR-T cells activity.** (**a**) Schematic representation of DARIC-1 targeting to the reverse
898 DNA strand of the *MTOR* locus, and DARIC-2 and 3 targeting to the *TRAC* locus using AAV6
899 donors. (**b**) Out-Out PCR for DARIC-1 knock-in detection at *MTOR* and DARIC-2 and 3 knock-
900 in at *TRAC*. Whole blood (WB) primary $CD3^+$ T cells were transfected with a SpCas9-G4 RNP
901 and transduced with AAV6 vectors with a multiplicity of infection (MOI) of $5x10^3$ for each AAV6.
902 Genomic DNA was harvested 3 days post-transfection. The percentage of edited alleles was
903 determined by TIDER from Sanger sequencing. Representative images are from one of two
904 independent biological replicates. (**c**) FACS-based cytotoxicity assay. $CD3^+$ T cells were
905 electroporated with *MTOR*/*TRAC* RNPs and transduced with both *MTOR*/*TRAC* AAV6 donors to
906 generate rapamycin-resistant (RapaR) CD19-CD22-DARIC-T cells. For rapamycin-sensitive
907 CD22-DARIC-T cells, the *MTOR* AAV6 donor was omitted. Three days post-nucleofection,
908 DARIC-T cells were incubated in the presence (rapamycin) or absence (vehicle) of 25 nM
909 rapamycin with NALM6 cells stably expressing RFP and K562-RapaR stably expressing EBFP
910 with an effector to target ratio of 1:1. Rapamycin-resistant NALM6 cells harboring the *MTOR*-
911 F2108L mutation (NALM6-RapaR) were used as a control to analyze the combinatorial impact of
912 rapamycin. The percentage of cytotoxicity was measured by FACS after 72 hours of incubation. *n*
913 = 2 independent biological replicates. Each data point represents the average of three technical
914 replicates.

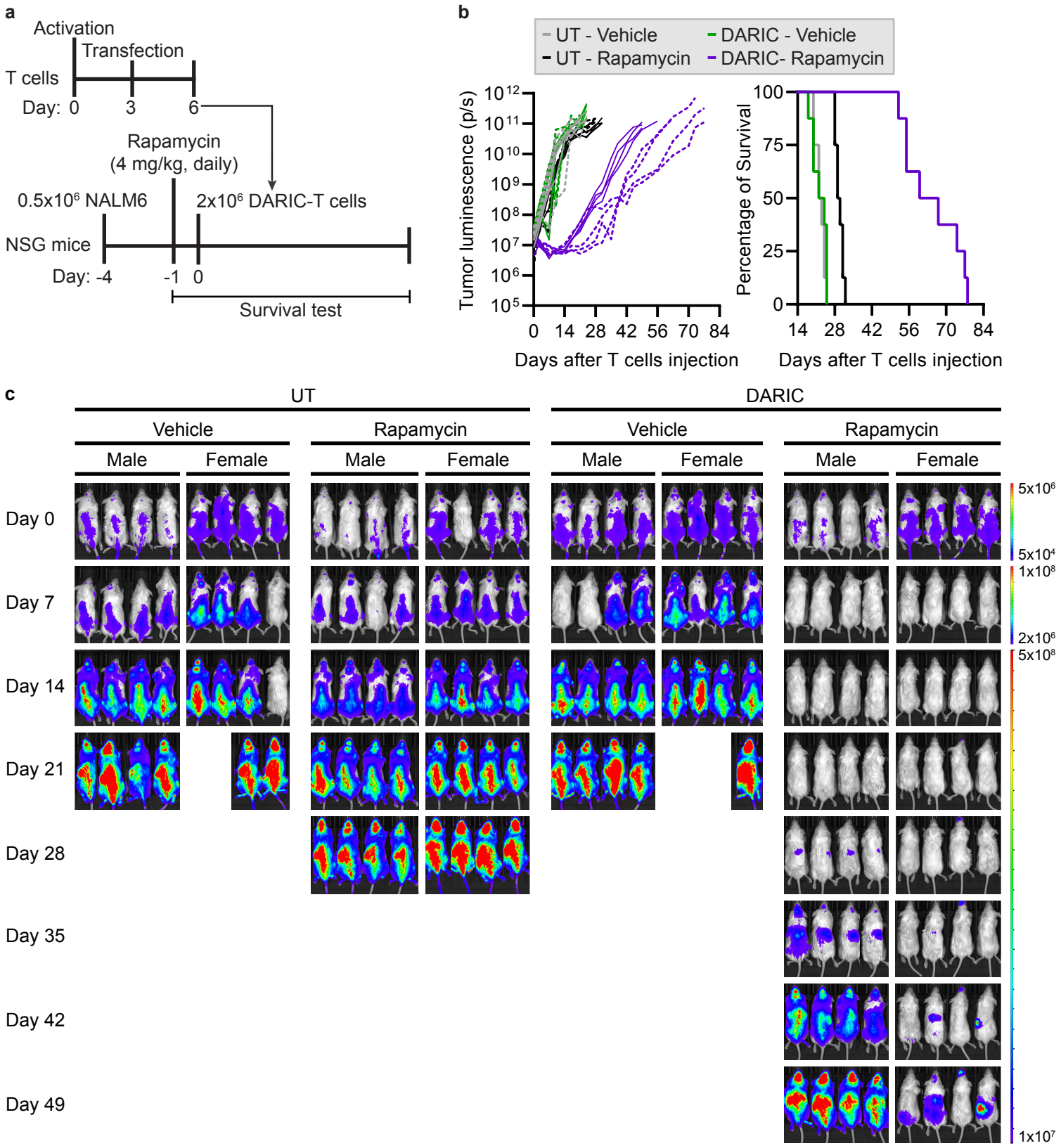

Figure 6
Levesque et al.

915 **Figure 6. Multiplexed DARIC targeting allows pharmacological activation *in vivo* with an**
916 **immunosuppressive dose of rapamycin.** (**a**) Timeline and experimental setup for the pre-B acute
917 lymphoblastic leukemia xenograft mouse model. Male and female NSG mice were challenged
918 with 0.5 x 10^5 NALM6-RFP-FLUC cells and daily rapamycin treatment (4 mg/kg) started three
919 days later. Four days after tumor inoculation, 2 x 10^6 untransduced (UT) T cells or DARIC-T cells
920 were injected. (**b**) Bioluminescence (BLI) quantification and Kaplan-Meier survival plot.
921 Leukemia engraftment, bio-distribution, and tumor progression were assessed by BLI imaging two
922 times per week. The radiance (photons/s) of the regions of interest (ROIs) corresponds to the area
923 containing the whole back side of the body. Radiance quantifications are illustrated with full and
924 dotted lines for male and female mice, respectively. n = 8 mice per group. (**c**) BLI and tumor bio-
925 distribution of all mice from (**b**) over seven weeks (See **Supplementary Fig. 8b** for tumor bio-
926 distribution over 11 weeks). The color barcode represents the radiance scale (photons/s/cm^2/sr).
927